Driving Advancements in the Mining Industry with Intelligent Solutions: Developing a Tool for Predicting the Unconfined Compressive Strength of Cemented Paste Backfill

Mariem Amri[1,3], Tikou Belem[1], Louis-Philippe Gélinas[2], Hatem Mrad[1], Faouzi Masmoudi[3]

[1]Université du Québec en Abitibi-Témiscamingue, Rouyn-Noranda, PQ, Canada, Mariem.Amri@uqat.ca; Tikou.Belem@uqat.ca; Hatem.Mrad@uqat.ca
[2]Agnico Eagle Mines Ltd, Rouyn-Noranda, QC, Canada, Louis-Philippe.Gelinas@agnicoeagle.com
[3]National School of Engineering of Sfax, Tunisia, faouzi.masmoudi@enis.tn

Abstract
Artificial intelligence (AI) stands as one of the most remarkable advancements in human history, finding applications across various sectors such as industry, healthcare, law enforcement, and finance. Despite its widespread integration, the mining industry, from exploration to exploitation, has been slow in fully utilizing the potential of AI. This is particularly evident in areas such as monitoring underground operations and detecting anomalies like seismic events and faults in mechanical systems. As the use backfill materials becomes crucial for mineral extraction, ongoing research challenges arise in comprehending and studying the diverse properties (mechanical, rheological, physical) of these materials. Cemented paste backfill (CPB) is the prevailing choice for mine backfill, with unconfined compressive strength (UCS) being a critical property defining its mechanical behavior. However, predicting the UCS of CPB remains a formidable challenge.

Exploiting the extensive big data generated by the mining industry provides an opportunity to create intelligent systems. This research aims to develop a smart tool utilizing Machine Learning (ML) and Deep Learning (DL) to predict the UCS of cemented paste backfills. To achieve this, a comprehensive dataset was compiled from Agnico-Eagle mines and supplemented with laboratory data, resulting in a rich database (DB) of 10,050 CPB specimens that encompass the physical, chemical, and mineralogical properties of ingredients. Prior to model training, an exploratory data analysis was conducted. Various intelligent models, including Random Forest (RF), Gradient Boosting Regressor (GBR), eXtreme Gradient Boosting Regressor (XGBR), and the Deep Neural Network (DNN), were employed. Based on performance indicators, the top-performing models, GBR and DNN, demonstrated coefficients of correlation (R) equal to 0.970 and 0.969, respectively. These models underwent validation in the laboratory through the preparation of new CPB mixtures. To make these models applicable for the mining industry, a user-friendly web application was developed, ensuring accessibility and ease of use for industry professionals.

Key words: artificial intelligence, database, prediction models, unconfined compressive strength, cemented paste backfill, web application

Introduction
Backfill has evolved into a crucial component of underground mine extraction, offering numerous economic and environmental advantages in Canada and globally (Brackebusch and Shillabeer, 1998; Fall et al., 2005; Orejarena and Fall, 2008). Particularly as a secondary support, it plays a vital role in maintaining the stability of underground excavations (Mitchell, 1989; Mitchell and Wong, 1982). CPB

stands out as the predominant choice in the mining industry, comprising mine tailings (70–85% solids content), a hydraulic binder (2–8% content) and mixing water. The mechanical properties, specifically the unconfined compressive strength, are significantly influenced by its ingredients, namely, the mineralogy, chemistry and physical properties of tailings, cement type and proportion, and water chemistry (Fall et al., 2005, 2004; Fall and Benzaazoua, 2005). Traditionally, UCS is predicted using conventional linear and non-linear regression methods based on experimental data (Arioglu, 1983; Lamos and Clark, 1989; Mitchell and Wong, 1982; Swan, 1985; Yu, 1989). However, achieving an accurate regression prediction with these empirical models is challenging. Moreover, these models are tailored to specific mines based on tailings type and do not encompass all the chemical, mineralogical and physical characteristics of CPB ingredients, limiting their generalizability.

In order to enhance the prediction of mechanical properties, it is crucial to transition from conventional regression methods to more sophisticated approaches. Currently, the talk is about the revolution of AI (Industry 4.0), a phenomenon evident in various manufacturing sectors. However, the mining industry has yet to embrace fully this technological advancement. Given the large amount of big data generated from mines, there is an opportunity to harness it for the development of intelligent systems. In this context, the objectives of this research study are to create intelligent models for predicting the UCS of CPB. However, several researchers have employed ML and DL models to forecast the UCS of CPB. Qi et al. (2023) trained a DNN of four hidden layers on a database containing 986 CPB specimens, considering the physical and chemical properties of the tailings, cement type, cement-to-tailings ratio, mass concentration, and curing time. The results show that the evolution of the network's loss function exhibits instabilities during training and the model gave a correlation coefficient of 0.967. Arachchilage et al. (2023), used ML models, namely GBR, RF, Support vector regression (SVR), and an Artificial Neural Network (ANN) with two hidden layers for UCS prediction based on literature and experimental data (307 CPB specimens), incorporating physical properties of tailings, chemical properties of cement, binder content, liquid-to-solid ratio, water-to cement ratio and curing time. The best-performing model was GBR, which gave a coefficient of determination of 0.96. In a study by Hu et al. (2022), the effect of temperature in alpine regions on the development of the UCS was investigated based on experimental data of 51 CPB samples, where they integrated sand-to-cement ratio, curing temperature, short-term curing time and slurry concentration as input variables to the ML model to predict UCS. The results demonstrate that low temperature (< 20°C) has the most significant effect on the hydration reaction process, and that the prediction model combined with the Sparrow Search Algorithm (SSA-ELM) achieved a correlation coefficient of 0.99. Additionally, other researchers have also developed intelligent models for predicting UCS of CPB (Lu et al., 2019; Sun et al., 2020).

While these studies play a crucial role in providing guidance, they are hindered by limitations that impede the effective adoption of ML or DL models. The databases used are often insufficient, containing < 2000 tests, limiting the development of intelligent models. Moreover, the studies overlook the simultaneous consideration of various factors affecting CPB strength, such as mineralogy, chemistry, physical properties of tailings, mixing water, binder type and proportion, solids mass concentration, slump, and curing time (long- and short-terms). Additionally, the performance of these models is not systematically evaluated by researchers. Furthermore, the overarching goal of developing intelligent models is to exploit their potential, yet their practical implementation as lines of code poses challenges for the industry. The emphasis in this research is on model development rather than addressing the operational hurdles

associated with integrating them into industry practices. Overall, these limitations underscore the need for a more comprehensive and practical approach in advancing the application of intelligent models in the field of mining engineering.

In addressing the limitations identified in the existing literature, we introduce an advanced tool designed for more accurate prediction of CPB strength. This entails leveraging a substantial database comprising 10,050 CPB specimens for the training of both ML models and a DNN. After training, model predictions undergo validation in a laboratory setting, allowing for comprehensive evaluation of their performance. Ultimately, a web application is crafted to operationalize the most robust model, ensuring practical and accessible utilization.

Materials and Methodology

Materials

In this investigation, five distinct types of tailings sourced from different mining companies (Agnico Eagle (LaRonde mine, Goldex mine, and Canadian Malartic mine), IAMGOLD (Westwood mine), and Hecla Quebec Mines (Casa Berardi mine)) were employed. These mine sites are situated in Abitibi-Témiscamingue in western Quebec, Canada (Figure 1). The tailings were transported in large 200 L barrels. The preparation process involved the initial removal of supernatant water, followed by meticulous homogenization to prevent particle segregation (Figure 2, step 1). Subsequently, the tailings were evenly portioned into 20 L plastic pails. Samples were extracted from these homogenized tailings and subjected to drying to ascertain their water content by weight (w%). Further deagglomeration and homogenization were performed using the four-point method. Relative density or specific gravity (G_s) was determined utilizing a helium pycnometer (ULTRAPYC 1200e), while particle size distributions (PSD) were analyzed using a Mastersizer 3000 laser diffraction particle size analyzer from Malvern Panalytical (Figure 2, step 2). Various binding agents, including GU, and blends of GU (ie., with Slag, type C fly ash, type F fly ash) were employed in conjunction with tap water and process water as a mixing water.

Methodology

The research methodology in this study comprises two parts. Initially, the focus is on laboratory work, starting with tailings homogenization and characterization as mentioned in the previous section. Subsequently, various backfill mixtures are prepared using these tailings, hydraulic binders, and mixing water (Figure 2, step 3). These mixtures are formulated using different binder ratios ($\%B_w = 100◌M_{binder}/M_{tailings}$) varying between 2–8%. and with various solids mass concentration ($\%C_w = 100◌M_{solids}/M_{bulk}$) ranging from 70–77%, aiming for a slump value between 5.75–10 in. (146–254 mm). The slump values are measured using the standard Abrams cone method, following the guidelines outlined in the ASTM C143 standard (ASTM International, 2020). The entire set of UCS data will be subsequently used for the development of ML models and a DNN in the later stages of the research.

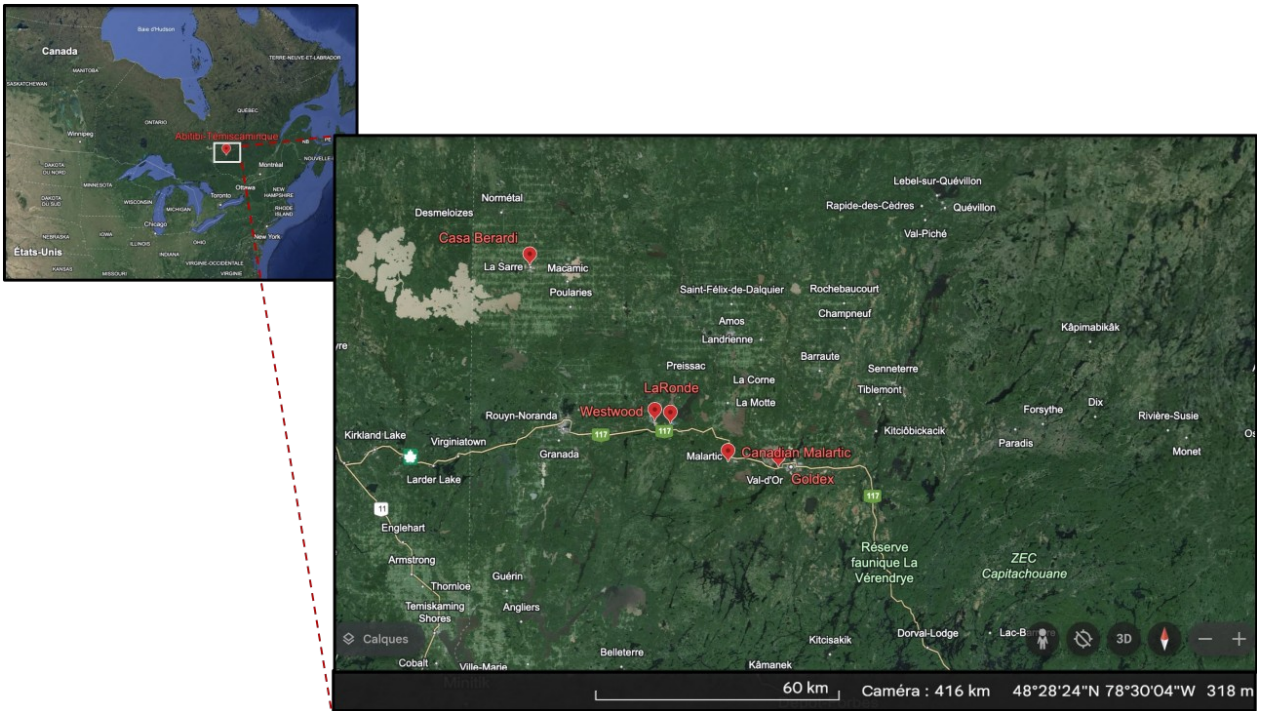

Figure 1. The five-mining site location in Abitibi-Témiscamingue.

In the laboratory experimental phase at the URSTM (Research and Service Unit in Mineral Technology) at UQAT, approximately 324 CPB specimens were manufactured. These specimens are then stored in a wet room with a controlled environment, maintaining a relative humidity higher than 90% and a temperature of 23°C±3° (Figure 2, step 4). After each curing time (7, 14, 28, 56, 90 and 105 days), the specimens underwent UCS tests using a stiff mechanical press MTS 10/GL with 50 kN maximum capacity while run at a constant displacement velocity of 1 mm/min in accordance with the ASTM C39 standard (ASTM International, 2021). The results of these tests allow determining the Uniaxial Compressive Strength (UCS) (Figure 2, step 5).

The latter part of this investigation focuses on the development and programming of ML and DL algorithms. Initially, the process commenced with data collection, incorporating laboratory results from 324 specimens and additional data obtained from various mines, for a total of 9726 specimens. The subsequent crucial step was exploratory data analysis (EDA). This encompassed addressing missing values in the databases, examining correlations among variables, normalizing them to ensure consistent scaling for optimal model learning, and annotating categorical data if required. Following the comprehensive processing of the database, it underwent a division into two segments: 80% of the data serves as the training set for model learning (development), while the remaining 20% constitutes the test set for model evaluation (validation).

The implementation of the models involves optimizing their hyperparameters. The evaluation of their performance guided by regression metrics, aids the selection of the most effective model. To validate operationalizing these models, a web application will be developed for user-friendly accessibility. The methodology adopted in this study is summarized in Figure 2.

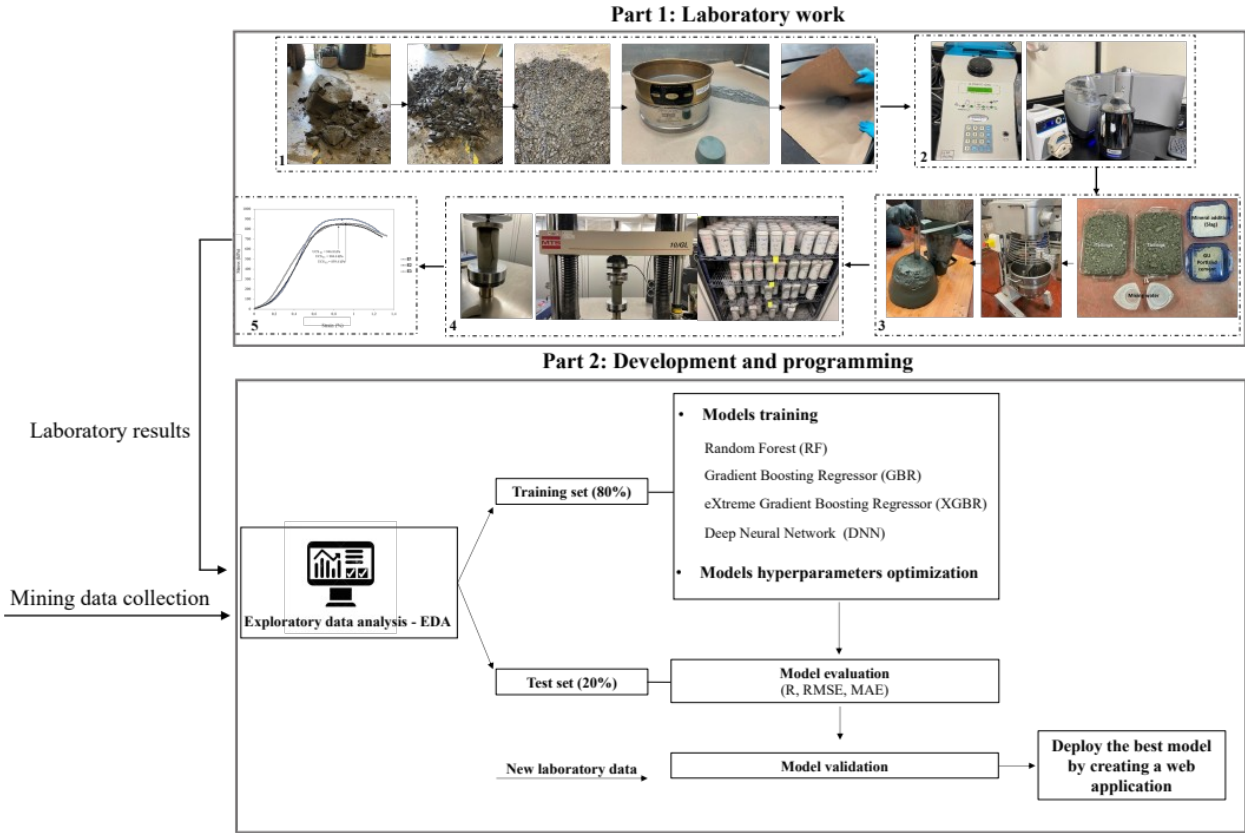

Figure 2. Methodology employed in the study.

Tailings characterisation

Figure 3 illustrates the particle size distribution of tailings, providing a means to assess their fineness. The curves depicted in the figure enable the evaluation of various tailings particle size parameters, as outlined in Table 1. Notably, the mine tailings fall within the silt particle size category. To obtain high paste backfill strength, it is essential for the tailings to exhibit well-graded particle size distribution. In our specific case study, the tailings exhibit a D_{10} ranging between 3–5 µm, a D_{50} between 18–40 µm, and a D_{90} between 87–165 µm. The uniformity coefficient (C_U) of tailings exceeds 2 (> 5), indicating a quasi-well-graded particle size distribution, potentially conducive to optimal performance.

Table 1. Physical parameters of tailings.

Origin of the tailings	w (%)	$\%C_w$	G_s	C_C	C_U	$P_{20\mu m}$ (d<20µm)
LaRonde mine	23.50	81.0	3.18	1.14	10.68	33
Westwood mine	23.39	79.1	2.82	1.15	7.03	48
Goldex mine	16.69	85.7	2.80	1.15	20.50	35
Canadian Malartic mine	20.30	83.1	2.76	1.07	9.79	42
Casa Berardi mine	23.10	81.2	2.97	0.83	8.93	51

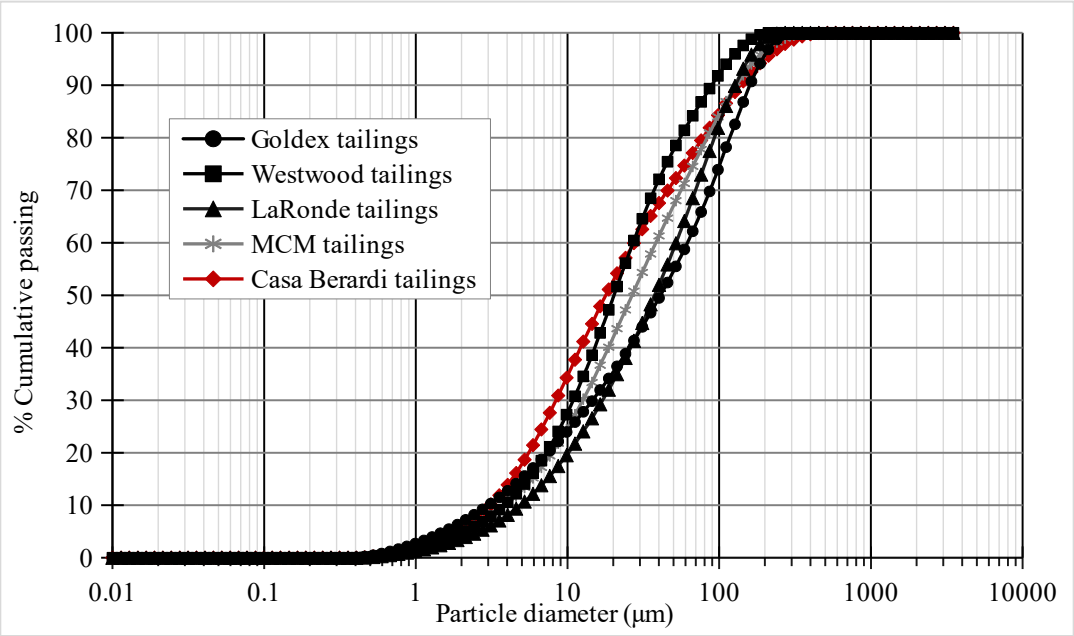

Figure 3. Particle size distribution of tailings samples.

Predicting UCS through intelligent methods

Exploratory Data Analysis (EDA)

Prior to initiating model training on the database, data processing is a prerequisite. Hence, this study undertook an exploratory analysis of the data. The initial phase involving addressing missing values, which were subsequently removed from the database. The second phase encompassed univariate, bivariate, and multivariate analyses. These analyses aimed to ascertain the frequency of each data item, comprehend the impact of one variable on another, and identify as well as assess the presence of outliers. A total of 6,750 CPB specimens were selected, focusing on key features encompassing the physical, mineralogical, and chemical properties of tailings, as well as parameters related to the mixture (eg, cement type, proportion, solids mass concentration, slump), chemical properties of the mixing water, and curing time.

Figure 4 depicts trends among selected data points on a two-dimensional plane, providing insights into their relationships. The point plots on the Cartesian plane do not reveal a distinct linear relationship.

However, the dashed red line signifies a regression estimate illustrating the association between these variables. These observed trends align with findings from previous studies (Belem et al., 2000; Fall et al., 2005, 2004).

Table 2 provides a statistical overview of all variables, revealing a substantial variance in standard deviation among them. This diversity poses challenges for model learning, creating complexities and hindering model convergence. Notably, the probability density function (Figure 6a) depicts a scattered distribution of the UCS variable, leading to the identification of outliers in Figure 5a. These outliers can significantly impact the performance of prediction models, as highlighted in previous studies (Nyitrai and Virág, 2019). To address this issue, data normalization is imperative to mitigate the adverse effects, as suggested by John (1995) and Osborne and Overbay (2004). Figure 6b illustrates a Gaussian distribution post-normalization, with fewer of the outliers evident in Figure 5b, achieved through the quantile transformation method.

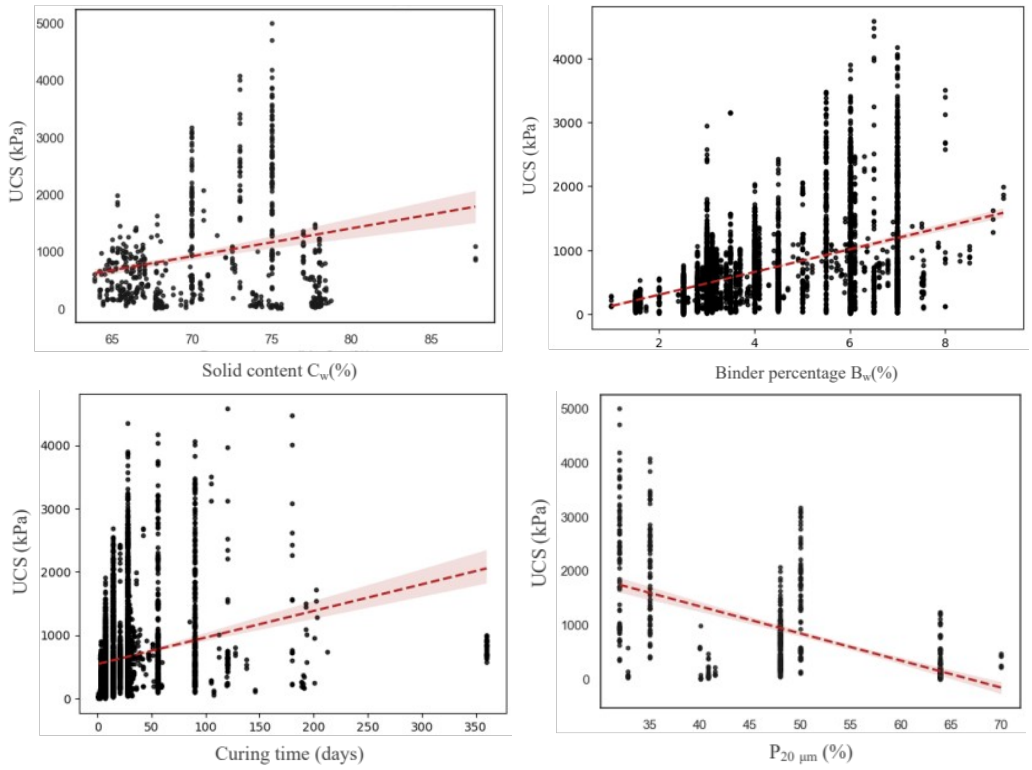

Figure 4. Trends between variables.

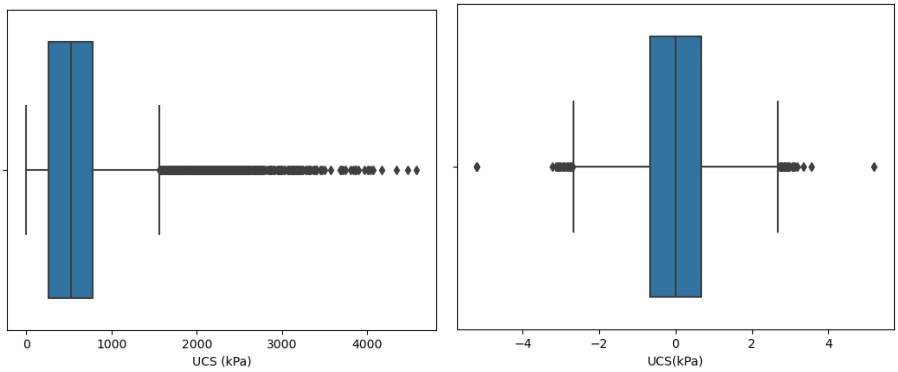

Figure 5. UCS Box plot: (a) before normalization, (b) after normalization

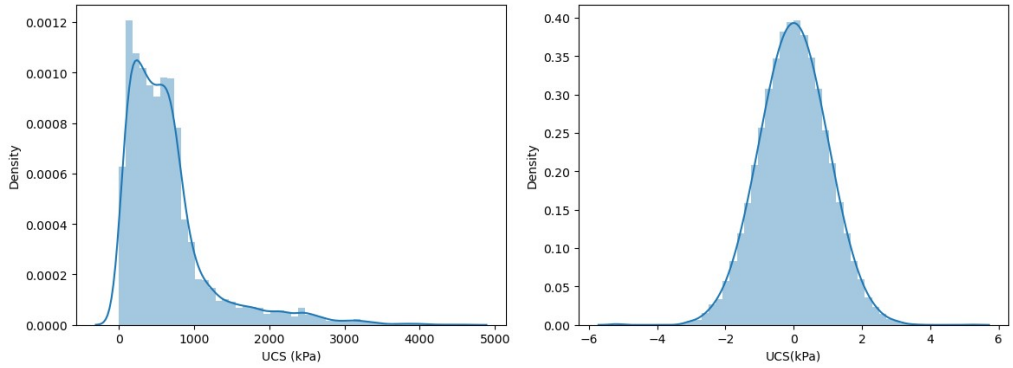

Figure 6. UCS probability density: (a) before normalization, (b) after normalization

Table 2. Statistical description of variables.

	Mean	**Std.**	**Min.**	**Max.**	**25th perc.**	**Median**	**75th perc.**
G_s	2.82	0.06	2.76	3.21	2.79	2.79	2.8
C_c	1.02	0.07	0.86	1.15	1.055	1.055	1.055
C_u	15.59	4.93	5.6	20.50	10.68	18.5	18.5
$P_{20\mu m}$ (%)	38.61	6.86	32	70	35	35	40
%Muscovite	7.66	7.65	0	40	4.38	4.38	4.38
%Other silicates	9.71	5.39	0	25.4	11.65	11.65	11.65
%Pyrite	1.66	4.12	0	27.5	0	0	2.68
%Other sulfides	0.19	0.72	0	3.28	0	0	0
Ca content (mg/kg)	31868.88	6743.47	4521	40696	32620	32620	32620
Mg content (mg/kg)	12012.92	3258.87	1823	14180	13780	13780	13780
S content (mg/kg)	10963.13	21509.66	2050	155000.00	2050	2050	16237
Zn content (mg/kg)	88.36	241.31	20	1313	20	20	89

Slump (po)	7.02	0.63	5	10	6	7	7
Solids content %C_w	74.57	2.31	63.9	93.45	74.6	75.3	75.7
GU Cement (%)	20.51	18.39	10	100	10	10	20
Fly Ash-C (%)	1.92	9.35	0	60	0	0	0
Fly Ash-F (%)	2.09	10.02	0	70	0	0	0
Slag (%)	75.47	27.64	0	90	80	90	90
Binder ratio B_w(%)	3.96	1.5	1	9.22	3	3.1	4.5
SO_4^{2-} in mixing water (mg/l)	498.92	1135.93	25	5000	171	171	171
SO_4^{2-} in tailings water (mg/l)	1825.67	196.45	1715	2355	1715	1715	1715
Curing time (days)	26.10	32.88	1	360	7	21	28
UCS (kPa)	649.94	594.18	0	4581	259.77	519.90	780.00

Considering factors such as data quality (categorical or tabular), data quantity (a substantial database for ML model training constraints), the number of features, and an unspecified data distribution, non-parametric ML models were selected for UCS prediction. In particular, the authors opted for RF, GBR, XGBR, and DNN, specifically a Feed-Forward Back Propagation Network (FFBPN).

RF

This algorithm is highly favoured in ML, employing multiple decision trees to form a forest. It utilizes the 'Bagging' technique, where each tree is trained on a random subset of the database. This approach justifies the name ‘Random Forest’. The predictions from all the trees are then combined by averaging, yielding a more robust and stable prediction compared to individual decision trees. By relying on bootstrapping to split the data, samples can undergo training multiple times on diverse decision trees, contributing to enhance performance. This model’s primary advantage lies in its capability to markedly diminish overfitting by averaging predictions from various trees, thereby surpassing the Decision Tree Regressor (DTR) in terms of generalization and flexibility. However, it comes with a computational drawback, being slower and less efficient for real-time predictions. Since its adoption, RF has proven valuable in addressing various prediction challenges. Applications range from predicting the slope stability to rock burst classification (Lin et al., 2018; Zhou et al., 2016), as well as tunnel-induced ground settlement analysis (Zhou et al., 2017).

GBR

Remaining a stalwart in ML, this algorithm has found extensive application in various engineering domains (Lu et al., 2019; Zhou et al., 2016). It operates by implementing forest trees and leveraging the 'Boosting' technique, constructing and training trees sequentially. Acknowledging the relatively low performance of each tree, the algorithm employs the 'Gradient Descent' optimization algorithm. This allows each tree to rectify the errors of its predecessor, creating a complementary model where the weaknesses of some trees are offset by the strengths of others. The algorithm initiates by forming a leaf containing the average value of the input on which it has been trained. Subsequently, it constructs the first tree, considering the prediction error of the initial leaf. Using the error from the first tree, GBR generates a new tree, repeating this process until the prediction error is minimized. This iterative approach systematically address prediction errors tree by tree, cumulating in the creation of a forest. The outcome for a new prediction is determined as the average prediction across all the trees. For a more in-depth understanding, refer to the detailed explanation provided by Friedman (2001).

XGBR

This algorithm is an optimized version of the GBR, designed to enhance both flexibility and efficiency. Like its predecessor, it relies on decision tree implementation and boosting. The process involves the sequential development of trees, with steps taken to reduce the error rate during successive iterations. The algorithm's initial step is training on the database to obtain an initial prediction. Subsequently, the residual (difference between the actual value and the predicted value), is calculated. The first tree is then constructed by training it on these residuals to minimize them. This process continues with the creation of additional trees until developing a tree no longer impacts the algorithm's performance. During the tree-building phase, the algorithm calculates a similarity score and output value for each decision node, aiming to enhance the performance of each tree.

The distinction between XGBR and GBR lies in the learning improvement mechanism. GBR relies on the first-order partial derivative (first-order gradient) of the loss function to adjust the learning process. In contrast, XGBR utilizes second-order gradients and incorporates the L1 and L2 regularization method to enhance model generalization (Chen and Guestrin, 2016). Due to this refinement in the learning process, XGBR is frequently observed to outperform GBR.

DNN

Artificial neural networks draw inspiration from the human brain, where numerous biological neurons process information. These neurons receive information through dendrites, transmit it as impulses along axons, and relay it to other neurons via synapses. In the context of predictive models, artificial neural networks comprise an input layer, hidden layers, and an output layer. All layers are interconnected, and neurons within the same layer operate independently. Each neuron is linked to preceding and subsequent neurons, featuring parameters such as weight, bias, and the threshold for information transmission.

In the supervised learning process adopted in this study, the neural network undergoes training through two primary steps: forward propagation and back propagation. Forward propagation involves passing input data from the first layer to the last, correlating inputs to outputs for the model training. At each layer, outputs (z) and associated activation functions ($a = f(z)$) for each neuron are calculated. Neurons compare the weighted sum of inputs with a threshold, delivering a response as output. Information transition between neurons, occurs via activation functions, facilitating the transformation of input data across the network. Back propagation adjusts the parameters of each neuron to minimize the loss function (model errors). This involves calculating partial derivatives relative to the weight (w_{ij}) and bias (b_i) of each layer. A comprehensive description of this calculation is available in (Amini et al., 2018; Grus, 2020; Shovic and Simpson, 2021). Figure 7 provides an illustrative example of a FFBP as used with a DNN.

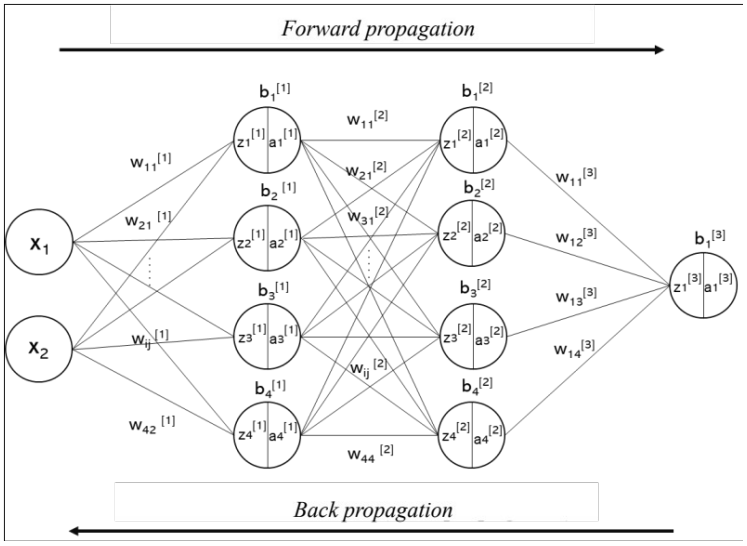

Figure 7. Illustration of the architecture of a FFBPN.

Results and discussion

Hyperparameters tuning

All ML models fall into two primary categories based on the nature of their parameters: parametric models and non-parametric models. Parametric models have predefined internal parameters before the learning process, while non-parametric models have external parameters that influence learning, known as hyperparameters. In our case study, the models are non-parametric, featuring a range of hyperparameters. Manually selecting values for each parameter can be intricate, and determining the optimal combination for the highest model score is even more challenging. To address this complexity, various processes are employed to search for these hyperparameters. This optimization step is crucial in the development of both ML and DL models. In this study, the authors identified optimal parameters for each model using the 'Randomized Search' method, followed by cross-validation. Tables 3a and 3b presents the optimal parameters for each model selected through this method.

Table 3a. Model optimal hyperparameters.

Model	Hyperparameters	Values
RF	Total number of trees in the forest (*n_estimators*)	1000
	The minimum number of samples required to split an internal node (*min_samples_split*)	2
	Maximum tree depth	15
GBR	Learning rate	0.2867
	Maximum tree depth	4
	The minimum number of samples required to split an internal node (*min_samples_split*)	2
	Total number of trees in the forest (*n_estimators*)	895

Table 3b. Model optimal hyperparameters.

Model	Hyperparameters	Values
XGBR	The portion of samples designated for fitting the individual base learners (subsample)	0.5
	Total number of trees in the forest (*n_estimators*)	400
	Maximum tree depth	6
	Learning rate	0.5
	The minimum loss reduction required to perform a split (*gamma*)	0
DNN	Number of hidden layers	4
	▪ First hidden layer	60 neurons
	▪ Second hidden layer	70 neurons
	▪ Third hidden layer	20 neurons
	▪ Fourth hidden layer	20 neurons
	Activation function	ReLU, tanh
	Learning rate	0.0001
	Optimizer	Adam
	Loss function	MSE

Model evaluation and comparison

In assessing the model quality, the authors employed statistical regression performance indicators, including:

Correlation coefficient (R)

This gauges the predictive quality of models by quantifying the relationship between predicted and actual values. The correlation coefficient ranges from 0–1, with a value nearing 1 signifying a well-fitting model capable of generalizing for accurate predictions. Conversely, a value close to 0 indicates a poor fit and, consequently, lower prediction quality. It is calculated using the following equation:

$$R=\frac{\sum_{i=1}^{N}(y_i^{¿}-\overline{y}^{¿})(y_i-\overline{y})}{\sqrt{\sum_{i=1}^{N}(y_i^{¿}-\overline{y}^{¿})^2}\sqrt{\sum_{i=1}^{N}(y_i-\overline{y})^2}} \quad \text{Equation 1}$$

The Root Mean Square Error (RMSE)

RSME k(Equation 2) serves as a pivotal performance metric for a predictive model specifically tailored for regression problems. When applied to a defined dataset, it calculates the root mean deviation between actual and predicted values. RMSE provides an estimation of the predictive model's proficiency in accurately predicting the target value.

$$RMSE=\sqrt{\frac{1}{N}\sum_{i=1}^{N}(y_i-y_i^{¿})^2} \quad \text{Equation 2}$$

The Mean Absolute Error (MAE)
MAE provides a comprehensive assessment of model error by measuring absolute errors. This approach ensures a holistic evaluation without penalizing errors, offering insight into the overall accuracy of the model.

$$MAE = \frac{1}{N}\sum_{i=1}^{N}\left|y_i - y_i^{¿}\right| \qquad \text{Equation 3}$$

where:

$y_i^{¿}$ = predicted values.
y_i = actual values.
$\overline{y_i^{¿}}$ and $\overline{y_i}$ = corresponding predicted and actual average values, respectively.

The curves depicted in Figure 8 compare the predicted values of each model with the actual UCS values on the test set, aligning along the 1:1 slope. This visual representation clearly illustrates model ability to generalize on new data when a good fit is evident on the slope. Among these models, GBR demonstrated the most optimal fit, evidenced by the highest coefficient of correlation (R) at 0.9701. In comparison, other models, RF, XGBR and DNN, yielded coefficients of correlation at 0.9588, 0.9635 and 0.9692, respectively. Examining the RMSE, GBR achieved a value of 0.2624, outperforming RF (0.2799), XGBR (0.2655), and DNN (0.0391).

(a)

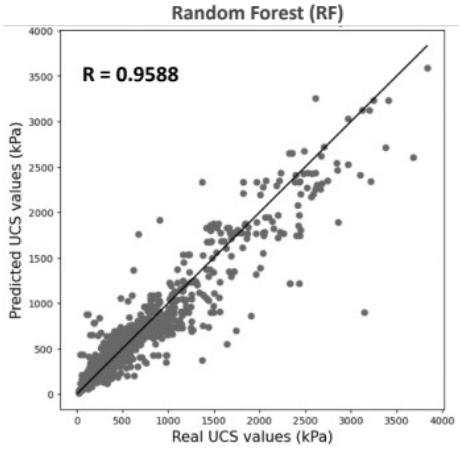

(b)

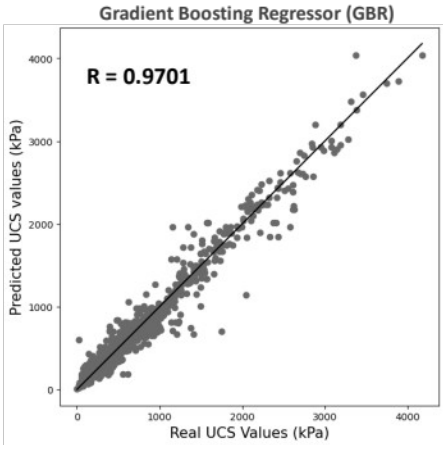

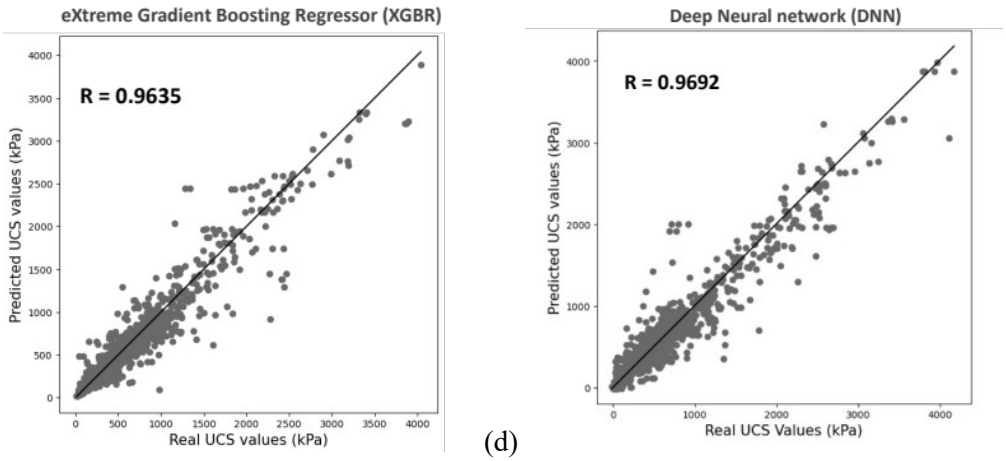

Figure 8. Model performance (a) RF, (b) GBR, (c) XGBR, (d) DNN

To enhance the evaluation of models, delving into their learning progress is crucial. Therefore, after model training, the database underwent k-fold cross-validation. This method involves randomly dividing the training dataset into k subsets, of which k-1 sets allocated for model training (training set) and one set for validation (validation set), as illustrated in Figure 9. In essence, the model is trained on the training set and evaluated on the validation set, generating a score each time. This cross-validation process iterates k times, with k set at 5 in this study. The significant advantage of this method lies in its ability to train the model multiple times, facilitating the improvement of its prediction score and mitigating the risk of model overfitting.

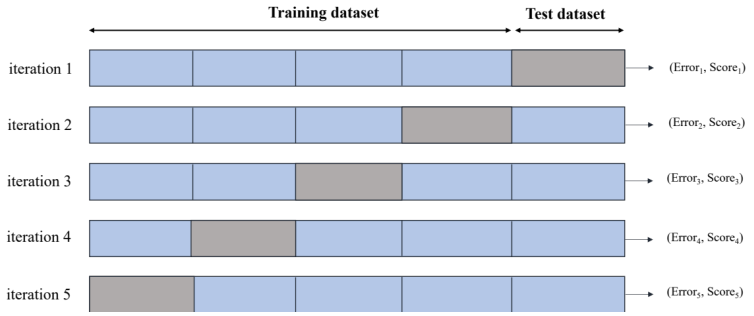

Figure 9. Scheme depicting the process of cross-validation.

Figure 10 illustrates the training performance of the models concerning the data to which they are exposed. Higher-quality data for model training typically results in improved performance. The blue curves depict effective learning on the training data, showcasing a slight decline in score as the data quantity increases. This decline is attributed to the challenges inherent in processing vast amounts of information. Notably, RF, GBR and XGBR models achieved high prediction scores of 0.92, 0.96 and 0.97, respectively. The green curves confirm the models' ability to generalize on new data, as the score

increases with learning progression. Noteworthy prediction scores (R) were recorded on the validation data, standing at 0.88, 0.92 and 0.91 for the RF, GBR and XGBR models, respectively. The minimal difference between prediction scores on the training and validation data, along with the convergence of these scores toward a stable point, attests to the models' good fit and their resilience against overfitting.

For more in-depth assessment of the DNN, the authors monitored the progression of its loss function, specifically the MSE, and its root, RMSE. Figure 11 illustrates that throughout the training process, both the MSE and RMSE decrease over a series of iterations, corresponding to the training data received. After a certain number of iterations, the error stabilizes not only for the training data but also for the validation data. It is crucial to note that the errors on the training data consistently remain smaller than those on the validation data, with minimal deviation between these two values. This observation validates the successful training of the DNN and the prevention of overfitting and underfitting.

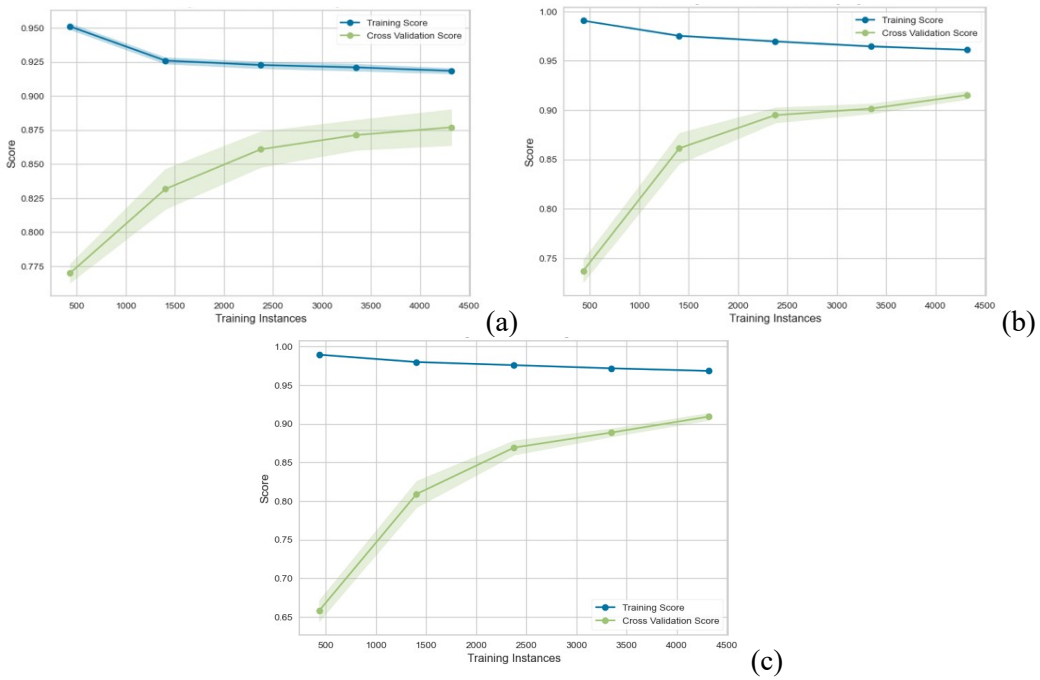

Figure 10. Learning curve of models (a) RF, (b) GBR, (c) XGBR.

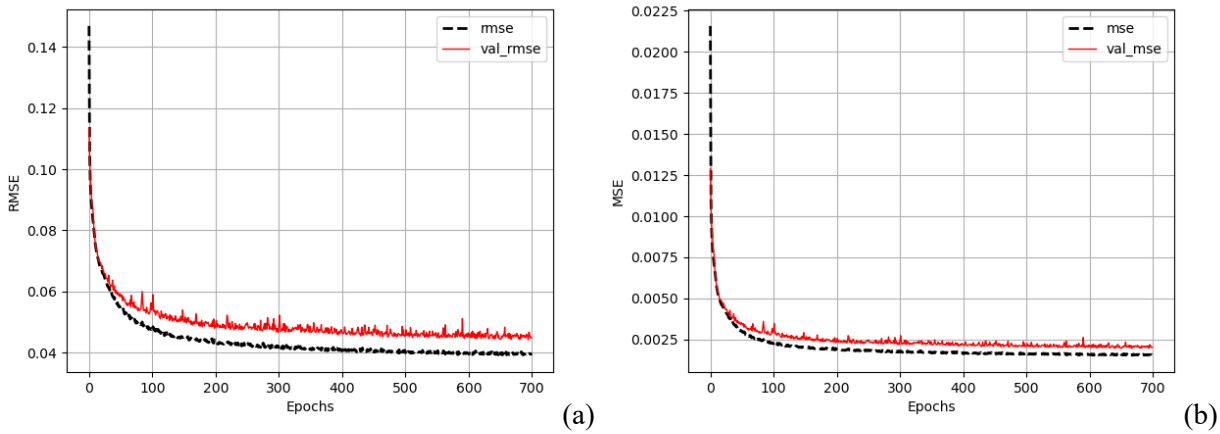

Figure 11. DNN performance evolution as a function of the number of iterations: (a) RMSE, (b) MSE.

Model Validation

To validate the models, eight CPB formulations (F_i, $i \in \{1,8\}$) were experimentally conducted in the laboratory, with these recipes absent from the database. The goal was to introduce entirely new data to the models, enabling them to make predictions for the corresponding UCS. Figure 12 provides a comparison between the predicted UCS from the models and the actual experimental UCS data. Among the models, the GBR demonstrated the closest alignment between predicted and actual UCS values, yielding the lowest MSE of 21.8 kPa. Following closely is the DNN, although it tends to overestimate the UCS with a MSE of 110.25 kPa. In third place is the XGBR, primarily associated with underestimation, presenting a MSE of 227.10 kPa. The RF model takes the last position, consistently underestimating with a MSE of 254.88 kPa. Figure 13 visually illustrates the prediction error of each model for the eight formulations, where negative errors indicate UCS underestimation and positive errors signify overestimation.

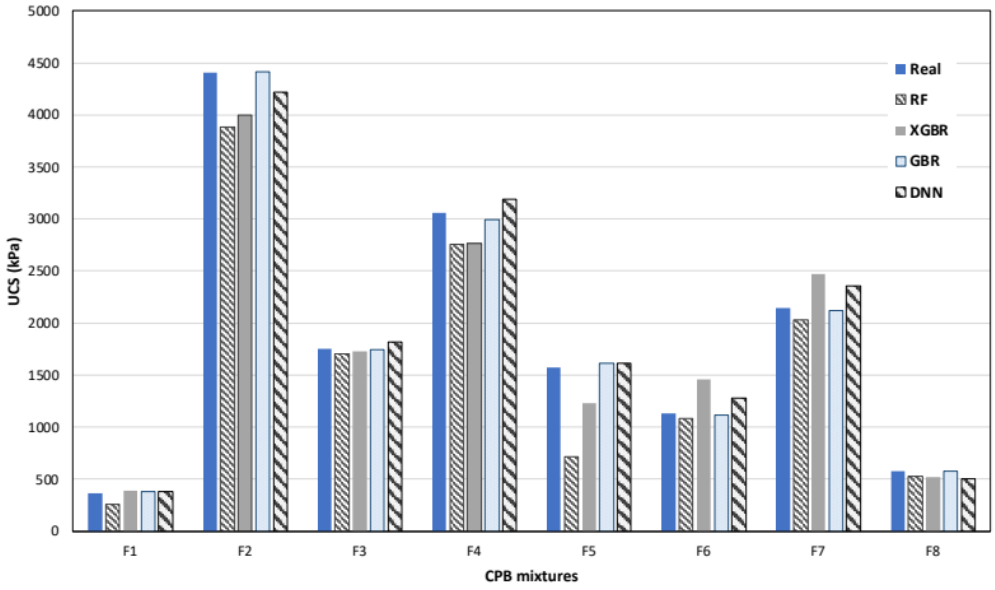

Figure 12. Comparison between predicted UCS values from models and the corresponding experimental results.

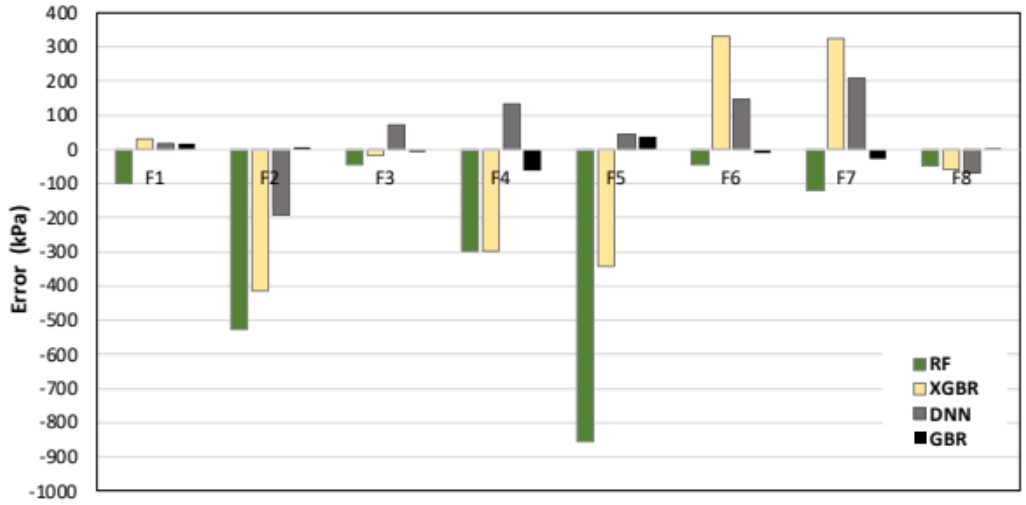

Figure 13. Model prediction errors.

Implementation of high-performance model for UCS prediction

While ML models and DNN, as lines of code, are not yet operational in the mining industry, there is a strong recommendation to develop tools for their practical use. This study contributes to this initiative by creating a web application, leveraging the GBR as the chosen and reliable model. The functionality of the application is outlined in Figure 14, allowing users to input the physical, mineralogical, and chemical characteristics of tailings, as well as mixing water properties, mixing parameters (binder type, proportion, solids mass concentration, slump), and curing time. Utilizing its learned patterns, the model predicts UCS, with the results displayed at the bottom of the figure.

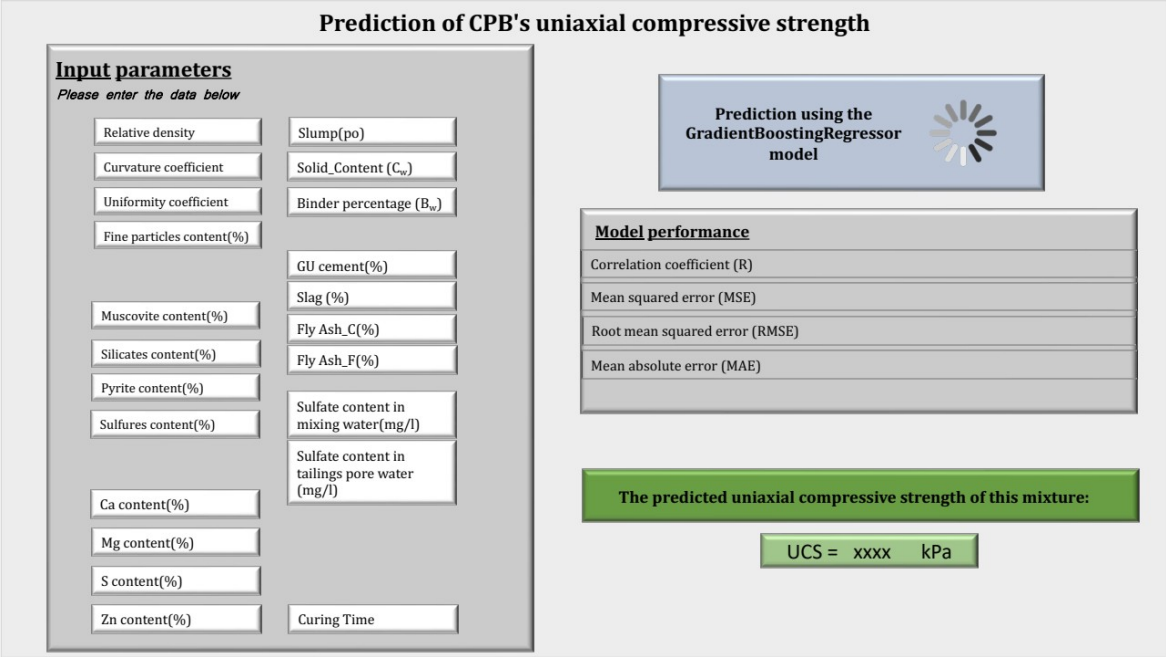

Figure 14. Intelligent UCS prediction tool.

Conclusion

This study involved the development of an intelligent tool employing ML algorithms and a DNN to predict the UCS of CPB. The prediction was based on a dataset encompassing laboratory experimental and mining UCS data, for a total of 10,050 CPB specimens. A comprehensive EDA preceded model training, with subsequent optimization of hyperparameters accomplished through the random search method followed by 5-fold cross-validation. Validation of model predictions was conducted both in the laboratory and through the utilization of performance indicators such as R, RMSE, MSE to assess their effectiveness. The derived conclusions are as follows:

- EDA has allowed for: 1) elimination of missing data from the database; 2) identification of arbitrary variable distributions and outliers, necessitating data normalization via the quantile transformation method; and: 3) identification of strong positive and negative correlations between variables, offering a comprehensive insight into the database.

- Learning curves of the models showcase their robust ability to generalize, demonstrating resilience against overfitting and underfitting.
- The GBR emerges as the most efficient model, providing a correlation coefficient (R) of 0.97.
- GBR has been implemented in a web application and is poised to become operational in the mining industry for UCS prediction.

Acknowledgement
The authors would like to express their sincere gratitude to the governments of Quebec and Canada for their financial support through (1) the Fonds de recherche du Québec-Nature et Technologie (FRQNT), Partnership Research Program on Sustainable Development of the Mining Sector II #2022-0MN-301195, (2) the Natural Science and Engineering Research Council of Canada (NSERC), Discovery Grant #RGPIN-2019-04946, and (3) Mitacs Accelerate Grant #IT38019- QC-ISDE. The authors would like to also thank AEM Ltd for its partnership and financial support through the Research Institute for Mines and Environment. A sincere thanks also go to Lafarge Inc. for providing GGBFS and Portland GU cement.

References

Amini, M.-R., Blanch, R., Clausel, M., Durand, J.-B., Gaussier, E., Cristophe Picard, J. M., Quéma, V., & Quénot, G. (2018). Data science. Eyrolles

Arachchilage, C. B., Fan, C., Zhao, J., Huang, G., & Liu, W. V. (2023). A machine learning model to predict unconfined compressive strength of alkali-activated slag-based cemented paste backfill. Journal of Rock Mechanics and Geotechnical Engineering, 15(11), 2803-2815. https://doi.org/10.1016/j.jrmge.2022.12.009

Arioglu, E. (1983). Engineering properties of cemented aggregate fill for Uludag tungsten mine of Turkey.

ASTM International. (2020). Standard Test Method for Slump of Hydraulic-Cement Concrete (ASTM C143/C143M-20), ASTM.

ASTM International. (2021). Standard Test Method for Compressive Strength of Cylindrical Concrete Specimens (ASTM C39/C39M-21).

Belem, T., Enzaazoua, M. B., & Bussière, B. (2000). Mechanical behaviour of cemented paste backfill. Rock Mechanics, 1.

Brackebusch, F., & Shillabeer, J. (1998). Use of paste for tailings disposal. In: Proceedings of the 6th international symposium on mining with back-fill (Minefill 98) AusIMM, publication no. 1/98, pp 53-58.

Chen, T., & Guestrin, C. (2016). XGBoost: A Scalable Tree Boosting System. Proceedings of the 22nd ACM SIGKDD International Conference on Knowledge Discovery and Data Mining, 785-794. https://doi.org/10.1145/2939672.2939785

Fall, M., & Benzaazoua, M. (2005). Modeling the effect of sulphate on strength development of paste backfill and binder mixture optimization. Cement and Concrete Research, 35(2), 301-314. https://doi.org/10.1016/j.cemconres.2004.05.020

Fall, M., Benzaazoua, M., & Ouellet, S. (2005). Experimental characterization of the influence of tailings fineness and density on the quality of cemented paste backfill. Minerals Engineering, 18(1), 41-44. https://doi.org/10.1016/j.mineng.2004.05.012

Fall, M., Benzaazoua, M., & Ouellet, S. (2004). Effect of tailings of paste backfill properties. International symposium Mine Fill.

Friedman, J. H. (2001). Greedy function approximation: A gradient boosting machine.

Grus, J. (2020). Data science par la pratique : Fondamentaux avec Python (2e éd). Eyrolles.

Hu, Y., Li, K., Zhang, B., & Han, B. (2022). Strength investigation of the cemented paste backfill in alpine regions using lab experiments and machine learning. Construction and Building Materials, 323, 126583.

John, G. H. (1995). Robust Decision Trees: Removing Outliers from Databases.

Lamos, A., & Clark, I. (1989). The influence of material composition and sample geometry on the strength of cemented backfill.
Lin, Y., Zhou, K., & Li, J. (2018). Prediction of Slope Stability Using Four Supervised Learning Methods. IEEE Access, 6, 31169-31179. https://doi.org/10.1109/ACCESS.2018.2843787
Lu, X., Zhou, W., Ding, X., Shi, X., Luan, B., & Li, M. (2019). Ensemble Learning Regression for Estimating Unconfined Compressive Strength of Cemented Paste Backfill. IEEE Access, 7, 72125-72133. https://doi.org/10.1109/ACCESS.2019.2918177
Mitchell, R. J. (1989). Stability of cemented tailings mine backfills. 501-508. http://pascal-francis.inist.fr/vibad/index.php?action=getRecordDetail&idt=7157900
Mitchell, R. J., & Wong, B. C. (1982). Behaviour of cemented tailings sands. 19: 289– 295.
Nyitrai, T., & Virág, M. (2019). The effects of handling outliers on the performance of bankruptcy prediction models. Socio-Economic Planning Sciences, 67, 34-42. https://doi.org/10.1016/j.seps.2018.08.004
Orejarena, L., & Fall, M. (2008). Mechanical response of a mine composite material to extreme heat. Bulletin of Engineering Geology and the Environment, 67(3), 387-396. https://doi.org/10.1007/s10064-008-0148-z
Osborne, J. W., & Overbay, A. (2004). The power of outliers (and why researchers should always check for them). https://doi.org/10.7275/QF69-7K43
Qi, C., Zheng, J., Yang, X., Chen, Q., & Wu, M. (2023). Application of deep neural network in the strength prediction of cemented paste backfill based on a global dataset. Construction and Building Materials, 391, 131827. https://doi.org/10.1016/j.conbuildmat.2023.131827
Shovic, J. C., & Simpson, A. (2021). Python tout en 1 pour les nuls. First interactive.
Sun, Y., Li, G., Zhang, J., Sun, J., & Xu, J. (2020). Development of an Ensemble Intelligent Model for Assessing the Strength of Cemented Paste Backfill. Advances in Civil Engineering, 2020, 1-6.
Swan, G. (1985). A new approach to cemented backfill design.
Yilmaz, E., Belem, T., Bussière, B., & Benzaazoua, M. (2011). Relationships between microstructural properties and compressive strength of consolidated and unconsolidated cemented paste backfills. Cement and Concrete Composites, 33(6), 702-715. https://doi.org/10.1016/j.cemconcomp.2011.03.013
Yu, T. (1989). Some factors relating to the stability of consolidated rockfill at Kidd Creek.
Zhou, J., Li, X., & Mitri, H. S. (2016). Classification of rockburst in underground projects: Comparison of ten supervised learning methods.
Zhou, J., Shi, X., Du, K., Qiu, X., Li, X., & Mitri, H. S. (2017). Feasibility of random-forest approach for prediction of ground settlements induced by the construction of a shield-driven tunnel.

Acronyms

CPB Cemented Paste Backfill
DL Deep Learning
DNN Deep Neural Network
FFBPN Feed-Forward Back Propagation Network
GBR Gradient Boosting Regressor
ML Machine Learning
RF Random Forest
UCS Unconfined Compressive Strength
XGBR eXtreme Gradient Boosting Regressor